Available online at www.sciencedirect.com
SCIENCE DIRECT
Atmospheric Environment 40 (2006) 5274–5297
ATMOSPHERIC ENVIRONMENT
www.elsevier.com/locate/atmosenv

Influence of the PBL scheme on high-resolution photochemical simulations in an urban coastal area over the Western Mediterranean

Carlos Pérez[a,*], Pedro Jiménez[a], Oriol Jorba[a], Michael Sicard[b], José M. Baldasano[a]

[a]*Barcelona Supercomputing Center-Centro Nacional de Supercomputación (BSC-CNS), Earth Sciences Division. Edificio Nexus II, C/ Jordi Girona, 29, 08034 Barcelona, Spain*

[b]*Department of Signal Theory and Communications, Lidar Group, Universitat Politècnica de Catalunya (UPC), C/ Jordi Girona 1,3, 08034 Barcelona, Spain*

Received 4 August 2005; received in revised form 11 April 2006; accepted 11 April 2006

Abstract

Planetary boundary layer (PBL) and land-surface processes have critical implications for air quality simulations. This contribution analyses the influence of three different surface/PBL schemes from the MM5 mesoscale meteorological model on the predicted photochemical pollutant concentrations using high-resolution EMICAT2000 emission model and Models-3/CMAQ chemical transport model. The Gayno–Seaman (GS), the Medium Range Forecast (MRF), and the Pleim–Chang (PC) PBL schemes are considered. The simulations focus on a complex coastal urban area (Barcelona Geographical Area) located in the Western Mediterranean for a typical summertime situation characterised by the absence of large-scale forcing. The particularities of the area require high spatial (1 km) resolution. Air quality, meteorological and lidar data are used for the evaluation of the results.

PBL height inputs have been considered as diagnosed by MM5 and re-diagnosed by the MCIP meteorological pre-processor of Models-3/CMAQ. Several variables playing an essential role in the concentrations of air pollutants, such as PBL height, temperature, and wind speed and direction, are analysed. Important differences are observed in GS scheme depending on the method used in the PBL height estimation. MRF and PC present similar results. Modelled daily maximum pollutants' concentrations vary in magnitude and location in function of the PBL scheme. GS–MM5 scenario presents the lowest PBL heights, the highest surface temperatures and the weakest winds during daytime, which provokes an enhanced O_3 formation. The higher concentrations of NO_x in the GS–MM5 scheme (which are caused mainly by the lower PBL height) provokes a higher depletion of O_3, which yields to the lower concentrations of this pollutant during nighttime in Barcelona downtown.

For regulatory purposes, the model tends to underestimate the photochemical formation in the area of study due to an underestimation of VOCs emissions in an VOC-limited area as Barcelona. The lower PBL height shown by GS taken from MM5, as well as the increase in the temperature and the weaker winds over coastal areas (that allow the accumulation of photochemical pollutants) promotes the O_3 concentration and improves the statistical scores of GS–MM5 scenario.

Keywords: Mixing height; Air quality modelling; MM5; Models-3/CMAQ; Complex terrain

*Corresponding author.
E-mail address: carlos.perez@bsc.es (C. Pérez).

1352-2310/$ - see front matter © 2006 Elsevier Ltd. All rights reserved.
doi:10.1016/j.atmosenv.2006.04.039

1. Introduction

The northeastern Iberian Peninsula (NEIP) has a complex topography with a large coast to the Mediterranean Sea. The complex configuration of the zone comes conditioned by the presence of the Pyrenees mountain range (with altitudes over 3000 m), the influence of the Mediterranean Sea and the large valley canalisation of Ebro River. The Barcelona area located in the NEIP is dominated by four main features arranged parallel to the coastline (Fig. 1): (1) the coastal plain, which comprises an 8-km strip of land between the sea and the first mountain range and which includes most of the cities in the greater urban area of Barcelona; (2) the coastal mountain range whose main peaks are Garraf, Collserola and Corredor, (3) the pre-coastal or Vallès depression, situated between the coastal mountain range; and (4) the pre-coastal mountain range. There are two main river valleys perpendicular to the coast: Llobregat and Besòs. The Llobregat and Besòs valleys contain highways and roads that link Barcelona and its outlying towns with the cities in the Vallès depression. Many industries are located around these urban areas as well as in the above-mentioned valleys.

In this area, the development of the breezes and mountain- and valley-induced winds have important effects in the dispersion of the pollutants emitted. The flow can be even more complex because of the land-use and the types of vegetation. Hence, the modelling of photochemical pollution in complex terrains demands a high horizontal spatial resolution (Jang et al., 1995; Jiménez et al., 2005a). In addition, boundary layer and land-surface processes have critical implications on air quality. Since meteorological fields are used as input to air quality models, it is well known that the treatment of the evolution and structure of the planetary boundary layer (PBL) in meteorological models has important implications for predicting and understanding the dynamics of ozone (O_3) and other photochemical pollutants (Zhang et al., 2001; Ku et al., 2001; Athanassiadis et al., 2002; Elleman et al., 2003; among others). The PBL has a thickness quite variable in space and time (from a hundred metres to a few kilometres) and its behaviour is determined by the dynamical and thermal forcing at the surface, synoptic divergence and advection and submittal entrainment. Under convective conditions, pollutants are emitted into the mixing layer (ML) and become gradually dispersed and mixed through the action of turbulence. The height of the ML or mixing height (MH) is a key parameter (Seibert et al., 1998).

The summer months in the region are characterised by the absence of large-scale forcing and the predominance of mesoscale circulations: the formation of a thermal low at a peninsular level forcing the convergence of surface winds from the coastal areas towards the central plateau with strong levels of subsidence over the WMB and sea–land breeze dynamics, which result in the re-circulation and accumulation of pollutants over the eastern Iberian coast (Baldasano et al., 1994; Millán et al., 1996, 1997; Soriano et al., 2001; Pérez et al., 2004; Jiménez and Baldasano, 2004). In the city of Barcelona, summer low MHs under unstable conditions (mainly limited to 400–800 m) are associated with large mesoscale compensatory subsidence over the sea and to the thermal internal boundary-layer (TIBL) formation at the coast (Sicard et al., 2006). The physical processes that govern the development of internal boundary layers are mechanically and thermally generated turbulent kinetic energy (TKE) within the layer, entrainment and subsidence aloft, and mesoscale advection through the layer. In photochemical model simulations, several important boundary-layer parameters for studying air pollution events are the MH, wind speed and direction, temperature and cloud cover.

This work analyses the influence of different surface/PBL parameterisation schemes from the Fifth Generation Penn State-NCAR Mesoscale Model (MM5) (Dudhia, 1993) and of the PBL height diagnosis on the predicted photochemical pollutant concentrations using the chemical transport model, Models-3/CMAQ (Byun and Ching, 1999). The results focus on a complex coastal area (Barcelona Geographical Area, BGA) located in the Western Mediterranean. High resolution (1 km) is applied in simulations to capture the complexity of the area. Meteorological, air quality and lidar measurements are used for evaluation of the results in this domain of study.The scenario analysed stands for an episode of photochemical pollution during 30 May 2002, which is characterised by the absence of large-scale forcing, the development of the Iberian thermal low and compensatory subsidence over the Western Mediterranean basin and breeze circulations over the area of study (Fig. 1).

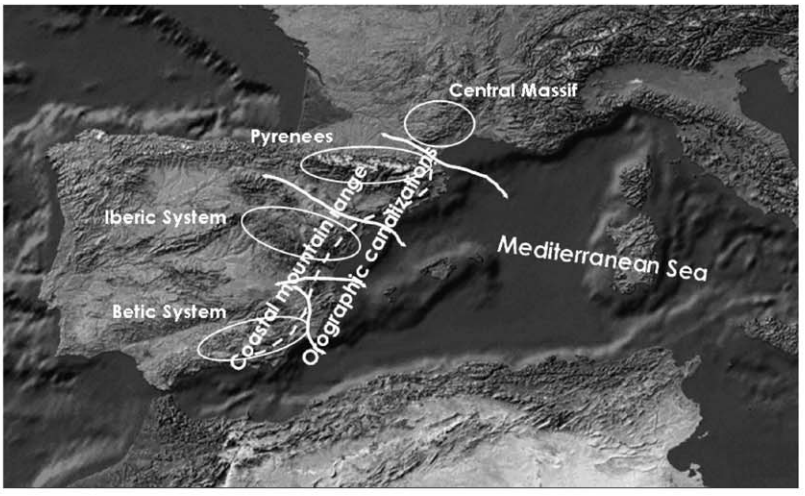
Central Massif
Pyrenees
Iberic System
Coastal mountain range
Orographic canalization
Mediterranean Sea
Betic System

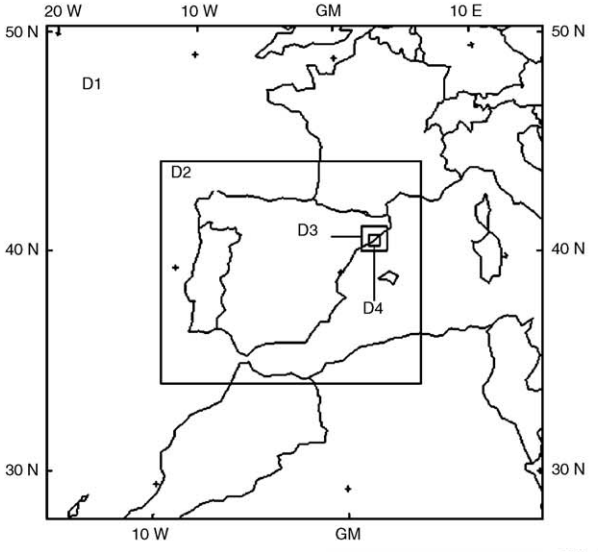
20 W
10 W
GM
10 E
50 N
40 N
30 N
D1
D2
D3
D4

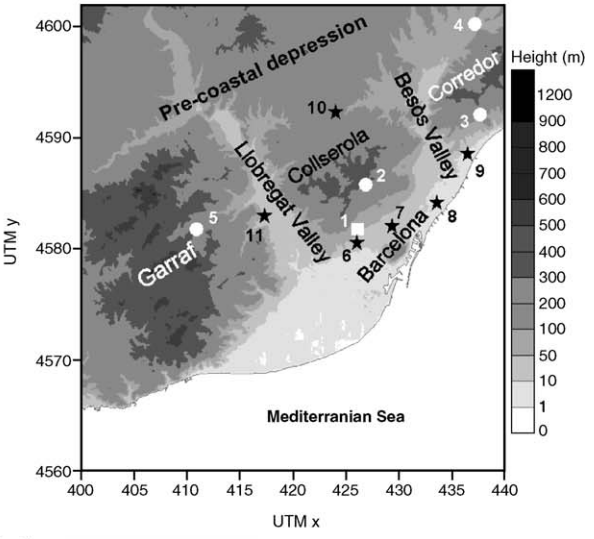
Pre-coastal depression
Besòs Valley
Corredor
Collserola
Llobregat Valley
Garraf
Barcelona
Mediterranian Sea
Height (m)
1200
900
800
700
600
500
400
300
200
100
50
10
1
0
UTM y
UTM x
4600
4590
4580
4570
4560
400
405
410
415
420
425
430
435
440

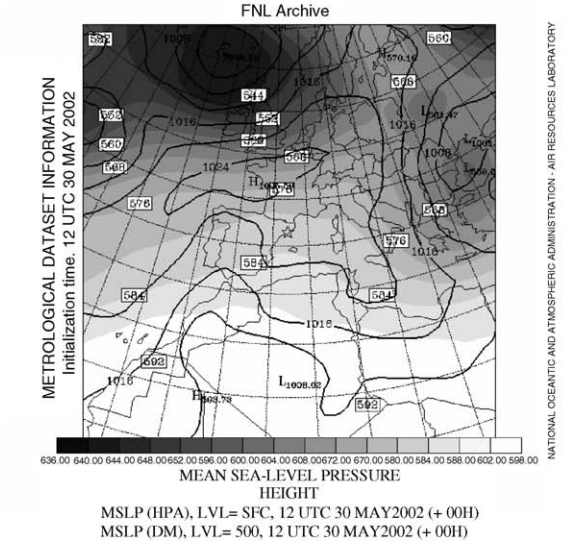
FNL Archive
METROLOGICAL DATASET INFORMATION
Initialization time. 12 UTC 30 MAY 2002
NATIONAL OCEANTIC AND ATMOSPHERIC ADMINISTRATION - AIR RESOURCES LABORATORY
MEAN SEA-LEVEL PRESSURE
HEIGHT
MSLP (HPA), LVL= SFC, 12 UTC 30 MAY2002 (+ 00H)
MSLP (DM), LVL= 500, 12 UTC 30 MAY2002 (+ 00H)

2. Methods

2.1. Models, land-surface/PBL schemes and MH calculation

Six base-case simulations are considered in this contribution, with PBL schemes considering both PBL diagnosis from MM5 and re-diagnosis from Models-3/CMAQ Meteorology-Chemistry Interface Processor (MCIP): the Gayno–Seaman (GS) scheme (Gayno, 1994) (GS–MM5, GS–MCIP), the Medium Range Forecast (MRF) (Hong and Pan, 1996) (MRF–MM5, MRF–MCIP) and Pleim–Chang scheme (PC) (Pleim and Chang, 1992) (PC–MM5, PC–MCIP). In order to account for the influence of temperature on air quality, an additional hypothetical scenario considers MRF parameterisation with an artificially modified temperature of +3 K in the entire troposphere (MRF + 3 K).

2.1.1. Meteorological model (MM5)

MM5 is a three-dimensional non-hydrostatic prognostic model. Four nested domains were selected (Fig. 1), which essentially covered southwestern Europe and North Africa (D1, 36 km resolution), the IP (D2, 9 km), the northeastern IP (D3, 3 km) and the domain of study: the Barcelona area (D4, 1 km). One-way nesting approach was used. The vertical resolution was of 29 σ-layers for all domains, the lowest one situated approximately at 10 m agl and 19 of them below 1 km agl. The upper boundary was fixed at 100 hPa. Initialisation and boundary conditions were introduced with final analysis data (FNL) of the National Weather Service's National Centers for Environmental Prediction (NCEP) Global Data Assimilation system (GDAS; Kanamitsu, 1989). The physics options used for the simulations were: the Kain–Fritsch cumulus scheme for D1 (Kain and Fritsch, 1993) and cumulus explicit resolution for D2, D3, and D4, all of them with no shallow convection, the Dudhia simple ice moisture scheme and the cloud-radiation scheme (MMMD/NCAR, 2001). Three PBL schemes are compared and evaluated. Each scheme is coupled to a different land-surface model, as described below:

1. The GS PBL coupled to the slab land-surface model: the GS local 1.5-order closure PBL scheme calculates TKE prognostically. The vertical diffusion coefficient is diagnosed based on the local value of TKE. The surface slab model based on the "force-restore" method developed by Blackadar (Zhang and Anthes, 1982) consists of an upper ground layer that is in contact with the atmosphere and a lower ground layer that has a specified, time-independent temperature. The GS scheme diagnoses the PBL height based upon the vertical TKE profile. During strong convection, the PBL height is set to the level where the maximum TKE falls below the critical value of $0.1\,m^2\,s^{-1}$; during weak convection, the PBL height is set to the level where the TKE is 50% of the maximum value. During periods of very weak turbulence, the PBL is set to the lowest model layer.
2. The MRF coupled to a five-layer soil model (Dudhia 1996): MRF is a non-local, first-order closure PBL scheme which consists of two regimes: a stable one based on non-local K-type closure theory and a free-convection regime which takes the contributions from large-scale eddies into account in the local, vertical mixing process throughout the PBL introducing the effect of entrainment at the top of the PBL to the mixing process. The scheme was initially developed for the MRF model, with relatively coarse horizontal and vertical resolution. The five-layer soil model predicts the ground temperature in 1, 2, 4, 8, and 16 cm layers with fixed substrate below using vertical diffusion equation. The transfer of heat follows the one-dimensional simple diffusion equation as the heat flux is linearly proportional to the temperature gradient. The PBL height diagnosis is based on the bulk Richardson number (Rib) method with a critical bulk Richardson number (Ribc) value of 0.5.
3. The PC PBL coupled to the Pleim–Xiu Land-Surface Model (Xiu and Pleim, 2001) is designed

Fig. 1. (Up) Orographic features of the Western Mediterranean Basin; (centre-left) nested domains were selected covering southwestern Europe and North Africa (D1, 36 km resolution), the IP (D2, 9 km), the northeastern IP (D3, 3 km) and the domain of study: the Barcelona area (D4, 1 km); (centre-right) location of meteorological stations (white circles), air quality stations (black stars), lidar, radiosounding and meteorological station (white square); (down) mean sea level pressure (contour lines) and geopotential height at 500 hPa (grey-shaded).

to simulate the characteristics of the land-surface vegetation and exchange with the PBL. The soil moisture model includes prognostic equations for soil moisture and soil temperature in two layers (1 cm and 1 m) as well as canopy water content. Surface moisture fluxes are modeled by three pathways: soil evaporation, evaporation and vegetative evapotranspiration. The PBL scheme is a simple non-local closure model called Asymmetrical Convective Model (ACM) developed specifically for application in regional or mesoscale atmospheric chemistry models. It is based on the concept that vertical transport within the ML is inherently asymmetrical. Upward transport by buoyant plumes originating in the surface layer is simulated by mixing from the lowest model layer directly to all other layers in the ML. Downward transport proceeds only to the next lower layer in order to emulate gradual compensatory subsidence. It computes the PBL height where Ribc = 0.25.

2.1.2. The Meteorology-Chemistry Interface Processor and the chemical transport model

The chemical transport model used to compute the concentrations of photochemical pollutants was CMAQ (Byun and Ching, 1999). The chemical mechanism selected for simulations was CBM-IV (Gery et al., 1989), including aerosols and heterogeneous chemistry. NO_x, VOC and PM speciation of EMICAT2000 emissions, as required by CBM-IV, could be found in Parra et al. (2006). Currently, the emissions of primary particulate matter in EMICAT2000 are under development, with the inclusion of dust re-suspension and loose material from paved roads. These emissions are essential for the characterisation of particulate matter in the Iberian Peninsula (Viana et al., 2005). Since this inventory has not been yet implemented, the analyses of aerosols have not been considered. The algorithm chosen for the resolution of tropospheric chemistry was the Modified Euler Backward Iterative (MEBI) method (Huang and Chang, 2001). With respect to dry deposition, the M3DDEP module (Pleim et al., 1996, 1997) has been used in all simulations. A further description of the MM5–EMICAT2000–CMAQ system and a full evaluation of its behaviour versus air quality data could be found in Jiménez and Baldasano (2004), Jiménez et al. (2005a, 2005b) and Parra et al. (2006). The MCIP essential role is to provide consistent meteorological data for the CMAQ modelling system (Byun et al., 1999).

MCIP allows either the direct pass through of the PBL parameters provided by MM5 (GS–MM5, GS–MRF and GS–PC scenarios), or they can be re-diagnosed using PBL similarity (GS–MCIP, MRF–MCIP and PC–MCIP scenarios). Basically, the re-diagnostic routines treat meteorological model outputs as the pseudo radiosonde observations. For unstable conditions, MCIP estimates the PBL height using the vertical profiles of potential temperature and the Rib (Holtslag et al., 1995). For stable conditions, the PBL height is determined by the maximum of the PBL height computed with the Rib and the stable boundary layer height given by Zilitinkevich (1989). The re-diagnostic algorithm could predict temporally disconnected PBL heights when the hourly meteorological data change abruptly. To minimise this effect, following limits on the PBL height are imposed: (1) compare with PBL height for neutral conditions, and take maximum; (2) compare with the urban boundary layer height. In MCIP, the minimum PBL height for urban area and other land-use types are set at 300 and 50 m, respectively; (3) limit the PBL height with a maximum value (3000 m) in case the temperature profile does not have a capping inversion. Although the radiation fields can also be re-diagnosed by MCIP, they have been introduced into CMAQ directly from input meteorology as estimated by MM5.

2.1.3. Emission model (EMICAT2000)

The high resolution (1 h and 1 km^2) EMICAT2000 emission model (Parra et al., 2006) has been applied in the northeastern Iberian Peninsula. This emission model includes the emissions from vegetation, on-road traffic, industries and emissions by fossil fuel consumption and domestic–commercial solvent use. Biogenic emissions were estimated using a method that takes into account local vegetation data (land-use distribution and biomass factors) and meteorological conditions (surface air temperature and solar radiation) together with emission factors for native Mediterranean species and cultures. On-road traffic emission includes the hot exhaust, cold exhaust and evaporative emissions using the methodology and emission factors of the European model EMEP/CORINAIR–COPERTIII (Ntziachristos and Samaras, 2000) as basis, and differencing the vehicle park composition between weekdays and weekends (Jiménez et al., 2005b). Industrial emissions include real records of some chimneys connected to the emission control net of

the Environmental Department of the Catalonia Government (Spain), and the estimated emissions from power stations (conventional and cogeneration units), cement factories, refineries, olefins plants, chemical industries and incinerators.

2.2. Measurements

The evolution of the ML was followed by means of an elastic lidar. Turbulent convective plumes transport aerosols from the surface. The relative differences between the aerosol in the ML and the clean air above are used to determine the MH (Boers et al., 1984). The lidar measurements presented in this paper were made at the Barcelona city (41.39°N, 2.12°E, 115 m asl, n.1 in Fig. 1) at a wavelength of 1064 nm on 30 May 2002. Sequences of 1-min duration (1200 shots) were recorded. A total of 16 packets of 30 sequences each were recorded between 0827 and 1940 UTC. For each packet of lidar profiles, the variance of the lidar profiles on each horizontal plane was calculated. The lowest altitude local maximum peak of the variance profile marks the ML mean depth. Therefore the variance method (VM) consists in finding the maximum of the variance of the 30 sequences of the range-squared-corrected signal (RSCS), i.e. the maximum of the variance profile:

$$h_{\mathrm{VM}} = \max_{z}\left[\operatorname*{Var}_{i=1,30}(\mathrm{RSCS}_i)\right] = \max_{z}\left[\frac{1}{30}\sum_{i=1,30}\left(\mathrm{RSCS}_i - \overline{\mathrm{RSCS}}\right)^2\right], \quad (1)$$

where $\overline{\mathrm{RSCS}}$ is the integrated profile of the whole packet. For each packet, the error bar, σ_{VM}, is calculated as the standard deviation of h_{VM} calculated couple of sequence by couple of sequence. The error bar is the standard deviation of the 15 vectors:

$$\left(\max_{z}\left[\operatorname*{Var}_{1,2}(\mathrm{RSCS}_i)\right], \max_{z}\left[\operatorname*{Var}_{3,4}(\mathrm{RSCS}_i)\right], \ldots, \max_{z}\left[\operatorname*{Var}_{29,30}(\mathrm{RSCS}_i)\right]\right).$$

Fig. 1 also shows the location of the radiosounding station measuring vertical profiles of temperature, specific humidity, wind speed and direction; the surface meteorological stations measuring temperature and wind speed and direction; and the air quality stations measuring O_3, NO_x and CO. The MH is defined by the height at which the condition Rib > Ribc is fulfilled (Holtslag et al., 1990). A value of 0.25 is taken for Ribc.

3. Results and discussion

The episode selected for the analysis and simulation of photochemical pollution (30 May 2002) corresponds to a typical summertime low-pressure gradient (Fig. 1) with high levels of photochemical pollutants over the Western Mediterranean. Under these conditions associated with weak synoptic forcing in the lower troposphere, mesoscale phenomena are dominant. The strong insolation promotes the development of prevailing mesoscale flows associated with the local orography (mountain and valley breezes), while the difference of temperature between the sea and the land in the coastal area enhances the development of sea–land breezes. The NEIP presents down-slope winds over the mountains and general weak offshore breeze flows at night. As the day advanced, a well-developed sea-breeze regime establishes along the entire eastern Iberian coast; this regime covered the central hours of the day. The onshore winds are well developed along the eastern coast, intensifying the anticyclonic circulation and deflecting to the east the flow between the Pyrenees and the Central Massif.

Table 1 depicts the O_3, CO and NO_x maximum and average concentrations according to different time-periods on 30 May 2002 (note that these concentrations refer to the whole domain of study and not to the air quality stations, that will be shown later). One can also observe that the concentrations of MRF and PC schemes (both derived from MM5 diagnose and MCIP re-diagnose) and GS–MCIP provide very similar concentrations and the only noticeable difference is observed in the case of GS–MM5 scenario.

3.1. Air quality evaluation of the different scenarios

Air quality station hourly data, averaged over the domain of study, were used to evaluate the performance of MM5–EMICAT2000–CMAQ predicting ground-level O_3, CO and NO_x for the different scenarios, both with PBL schemes diagnosed with MM5 and re-diagnosed with MCIP. Hourly measurements of ambient pollutants were provided by air quality surface stations in the domain of study, which are part of the Environmental Department of the Catalonia Government (Spain).

The US Environmental Protection Agency has developed guidelines (US EPA, 1991) for a minimum set of statistical measures to be used for the

Table 1
Intercomparison between the six scenarios of O_3 ($\mu g\,m^{-3}$), CO ($mg\,m^{-3}$) and NO_x ($\mu g\,m^{-3}$) maximum and average concentrations according to different time-periods in the whole domain of study of the Barcelona Geographical Area

	GS (MM5)	GS (MCIP)	MRF (MM5)	MRF (MCIP)	PC (MM5)	PC (MCIP)
Maximum 1-h concentration						
O_3 ($\mu g\,m^{-3}$)	119.25	115.40	112.56	111.19	109.35	111.17
CO ($mg\,m^{-3}$)	1.06	0.96	1.04	0.92	0.90	0.87
NO_x ($\mu g\,m^{-3}$)	259.49	218.55	297.28	273.09	244.87	222.30
Maximum 8-h average concentration during daytime						
O_3 ($\mu g\,m^{-3}$)	74.67	78.81	77.85	76.85	77.07	76.71
CO ($mg\,m^{-3}$)	0.15	0.11	0.10	0.10	0.10	0.10
NO_x ($\mu g\,m^{-3}$)	20.19	11.95	8.11	9.99	8.33	9.18
Daily average concentration						
O_3 ($\mu g\,m^{-3}$)	58.96	62.55	61.15	60.67	58.12	58.48
CO ($mg\,m^{-3}$)	0.19	0.16	0.15	0.15	0.16	0.16
NO_x ($\mu g\,m^{-3}$)	29.96	24.25	21.69	22.61	23.49	24.29

evaluation of O_3 in regions where monitoring data are sufficiently dense. These statistical measures considered are the mean normalised bias error (MNBE); the mean normalised gross error (MNGE) for concentrations above a prescribed threshold, and the unpaired peak prediction accuracy (UPA). In addition, the European Directive 2002/3/EC related with O_3 in ambient air assumes an uncertainty of 50% for the air quality objective for modelling assessment methods. This uncertainty is defined as the maximum error of the measured and calculated concentration levels during daytime.

Table 2 summarises the results of the statistical analysis. Although there is no criterion for a "satisfactory" model performance in the case of O_3, US EPA (1991) suggested values of $\pm$10–15% for MNBE, $\pm$15–20% for the UPA and +30–35% for the MNGE to be met by modelling simulations, to be considered for regulatory applications.

The performance objective in the Directive 2002/3/EC (deviation of 50% for the 1-h averages during daytime) is achieved for the entire period of study for all schemes within MM5–EMICAT2000–CMAQ. The O_3 bias of the different schemes is negative on each day of the simulation, progressively increasing from −9.1% in the scenario of MRF with modified temperature until −14.8% on PC–MCIP. This overall negative bias may suggest that the O_3 production chemistry in MM5–EMICAT2000–CMAQ may not be sufficiently efficient. According to Jiménez and Baldasano (2004), the underestimation of O_3 levels in the area of study may be caused by an underestimation of VOC emissions on the VOC-limited area of BGA.

Table 2
Results of the evaluation of O_3, CO and NO_x with MM5–EMICAT2000–CMAQ models against data from air quality stations located in the domain of Barcelona Geographical Area

	MNBE (%)	RMSE ($\mu g\,m^{-3}$)	MNGE (%)	UPA (%)
Ozone (O_3)				
GS MM5	−9.9	18.8	19.7	3.9
GS MCIP	−10.1	20.1	20.1	−19.6
MRF MM5	−12.2	23.4	23.0	−22.1
MRF MCIP	−14.1	22.1	22.8	−22.6
PC MM5	−12.2	20.7	22.8	−24.7
PC MCIP	−14.8	21.6	24.6	−24.7
Carbon monoxide (CO)				
GS MM5	12.6	0.22	53.4	2.4
GS MCIP	−4.3	0.19	40.8	−8.9
MRF MM5	−12.7	0.23	42.1	−16.5
MRF MCIP	−4.0	0.18	34.1	−19.5
PC MM5	−18.4	0.23	45.4	−16.1
PC MCIP	−5.3	0.21	43.3	−18.8
Nitrogen oxides (NO_x)				
GS MM5	12.6	37.9	26.9	−3.5
GS MCIP	−11.1	60.8	26.2	−44.7
MRF MM5	−2.6	66.4	34.4	−40.4
MRF MCIP	−10.2	63.0	23.4	−58.4
PC MM5	−7.8	60.7	28.6	−29.8
PC MCIP	−7.3	64.3	26.3	−43.5

However, US EPA goals of $\pm$15% are achieved by all parameterisations and scenarios included.

The MNGE ranges from 19.7% for GS–MM5 to 24.6% for PC–MCIP. This error is strongly related to the root-mean-square error (RMSE), that varies from 18.8 $\mu g\,m^{-3}$ for GS–MM5 to 23.5 $\mu g\,m^{-3}$ in MRF–MM5. However, the MNGE derived from

the results achieve the US EPA goals for a discrete evaluation of all the scenarios (<35%).

Figs. 2, 3 and 4 indicate the evaluation of the model for the locations of several air quality stations placed in different environments of the modelling domain, as shown in Fig. 1. The measured O_3 1-h peak concentration in the area of study (115 μg m^{-3}) (Fig. 2, down) is well captured by all parameterisations, with values ranging from 119 to 86 μg m^{-3} in the case of GS–MM5 and PC (both diagnosed and re-diagnosed), respectively. However, the results of the simulations with the different schemes indicate that modelled concentrations appear at different regions of the domain according to the parameterisation of the PBL scheme. The time of occurrence of maximum O_3

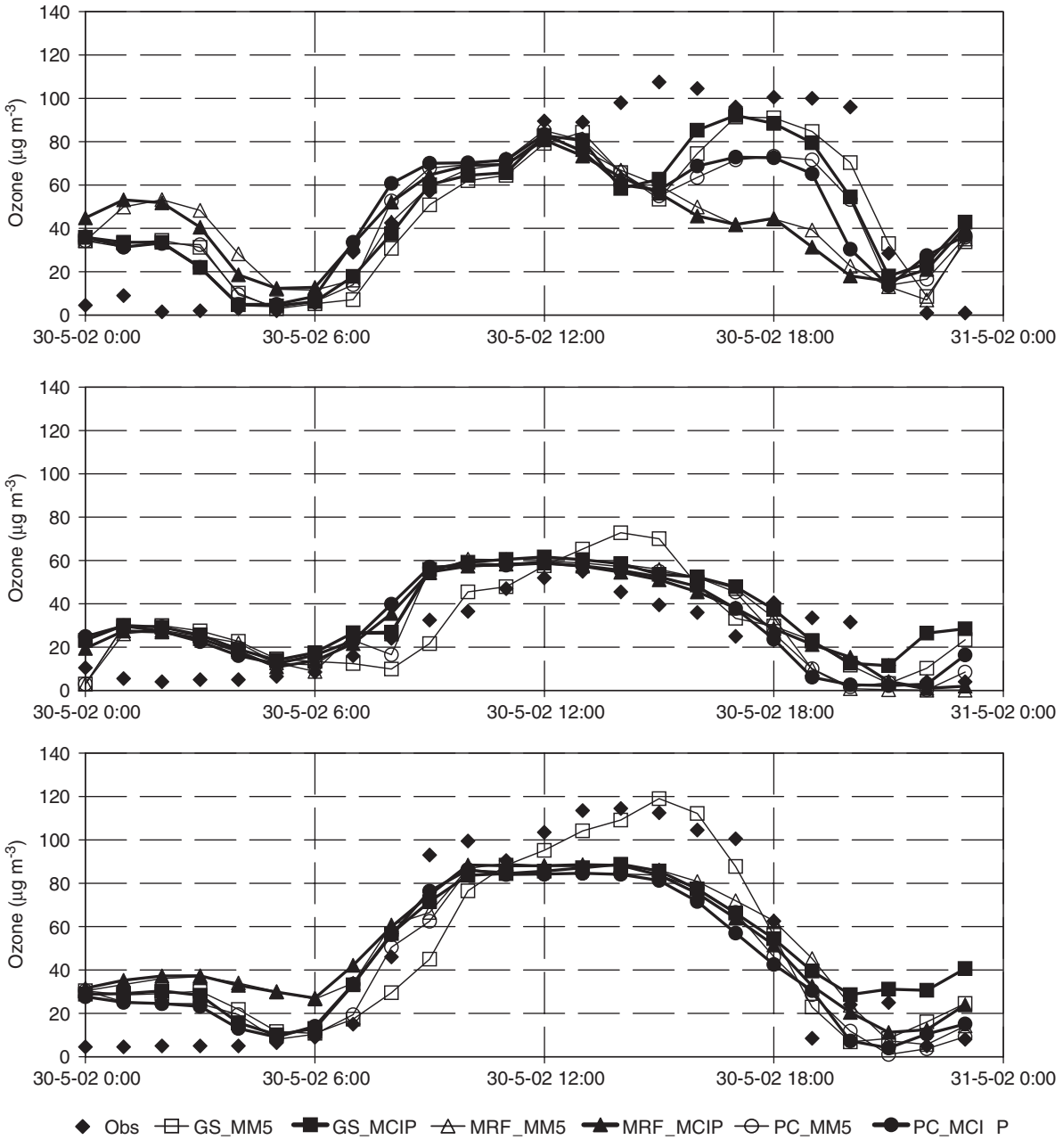

Fig. 2. Measured (solid diamonds) and simulated O_3 ground levels (μg m^{-3}) with the different PBL schemes in locations of the domain of study: (up) Badalona (n.9 in Fig. 1), (centre) Barcelona–Eixample (n.7) and (down) Sant Cugat (n.10).

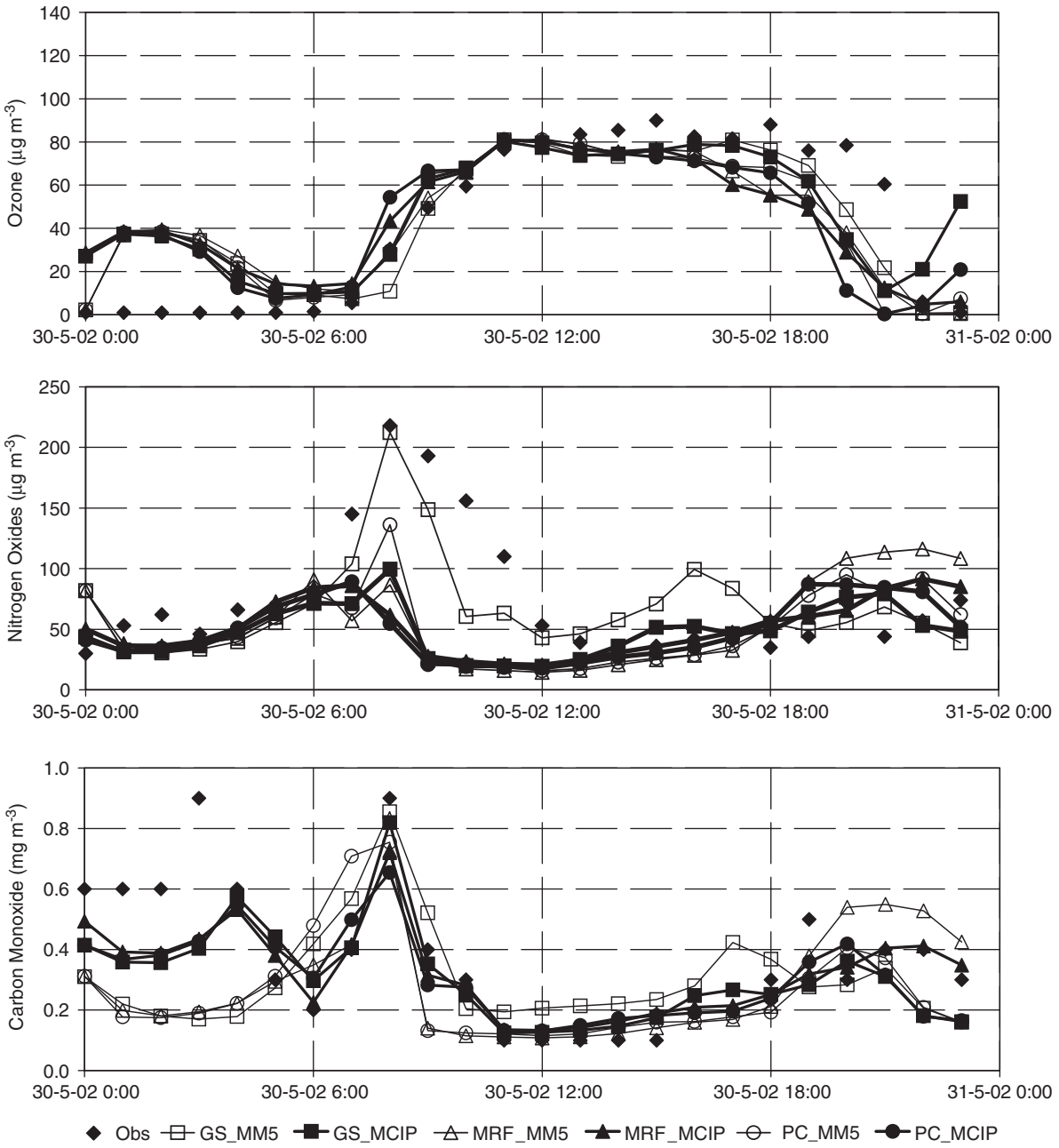

Fig. 3. Measured (solid diamonds) and simulated ground levels of (up) O_3 ($\mu g\,m^{-3}$), (centre) NO_x ($\mu g\,m^{-3}$) and (down) CO ($mg\,m^{-3}$) with the different PBL schemes in Barcelona–Poblenou (n.9 in Fig. 1).

levels at a given cell or region can differ by several hours. In addition, differences in the predicted peak O_3 concentrations during daytime for a determined hour of the day can be higher than $40\,\mu g\,m^{-3}$.

Fig. 2 also shows that the GS–MM5 presents a more marked cycle of O_3 during daytime in the stations located in different parts of the area of study: Badalona (n.9 in Fig. 1), Barcelona–Eixample (n.7), Sant Cugat (n.10). They present a slower formation of this photochemical pollutant (with higher and later 1-h peak concentrations with respect to other parameterisations) and a more rapid depletion in the afternoon and nighttime hours in Barcelona–Eixample and Sant Cugat. The UPA is negative during the simulated episode for all the scenarios, except in the case of GS–MM5

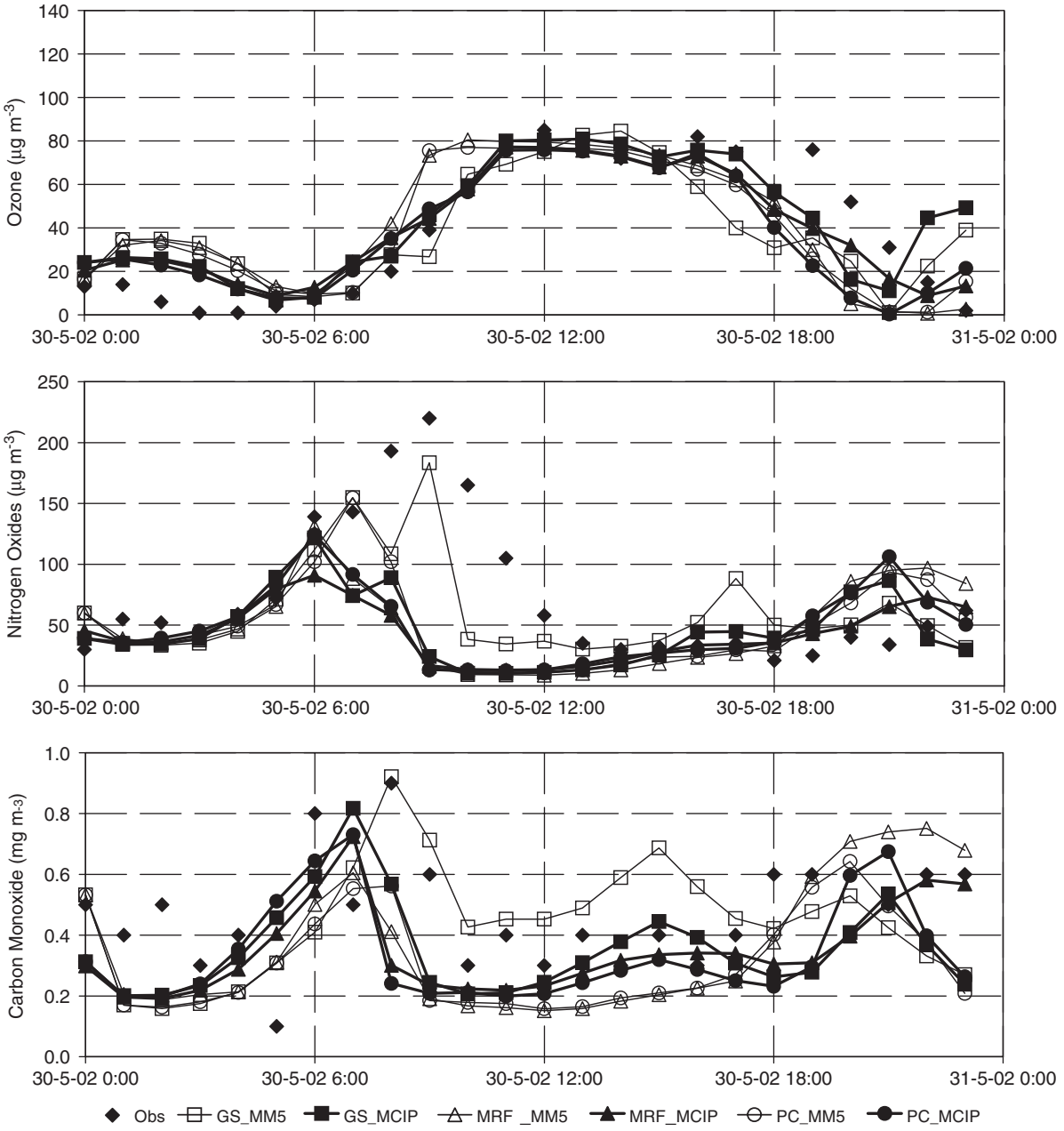

Fig. 4. Measured (solid diamonds) and simulated ground levels of (up) O_3 ($\mu g\,m^{-3}$), (centre) NO_x ($\mu g\,m^{-3}$) and (down) CO ($mg\,m^{-3}$) with the different PBL schemes in L'Hospitalet de Llobregat (n.6 in Fig. 1).

(+3.9%). The underprediction ranges from −19.6% in GS–MCIP to −24.7% for PC scheme.

Table 2 also presents the results of the evaluation of simulations with different statistical parameters for CO and NO_x. On-road traffic is the main source of CO and NO_x precursors at this domain. The strong morning peak of these precursors observed in Figs. 3 and 4 can be explained from the following considerations: emissions are high coinciding with the morning rush hour, the MH is still small and winds are weak due to the morning sea-breeze transition. On-road emissions are slightly reduced after the morning rush hour, the PBL grows and the sea breeze intensifies diluting and advecting pollutants. In the afternoon, the influence from traffic emissions is coupled to the cooling of the

atmosphere and large mesoscale compensatory subsidence, which result in an increase in the concentration of pollutants. The simulations for these photochemical pollutants tend to show larger biases and errors than the corresponding statistics of O_3 for the same simulation. As noted by Russell and Dennis (2000), current air quality models have a pervasive tendency towards the underprediction of O_3 precursors.

In the case of CO and NO_x, the mean bias is negative for all scenarios (ranging from −4.0% to −18.4% in the case of CO and −2.6% to −11.1% for NO_x) except in the case of GS–MM5, where MNBE is +12.6% for CO and NO_x. The same behaviour is observed for the peak accuracy. As observed in Table 2 and Figs. 3 and 4 for different locations within the domain, the 1-h peak is clearly underestimated in all the scenarios for CO (ranging from −8.9% for GS–MCIP to −19.5% for MRF–MCIP) and NO_x (−29.8% for PC–MM5 to −58.4% for MRF–MCIP) except in the case of considering GS–MM5 (positive UPA of 2.4% for CO and −3.5% for NO_x). However, this accuracy in the prediction of the peak is not corresponded to the gross error. The tendency to overprediction is reflected in the MNGE for CO (53.4% for GS–MM5, higher than other parameterisations, that yield values around 40%). The lowest MNGE for these precursors is observed for MRF–MCIP, which at the same time presents the highest UPA error (−19.5% for CO and −58.4% for NO_x).

Below we include an analysis of the modelled differences according to the main variables that can play an important role in the concentration of photochemical pollutants and that are considered differentially in the PBL schemes.

3.2. Influence of PBL parameters on air quality

3.2.1. Mixing height

The diurnal cycle of the MH over the city of Barcelona on 30 May 2002 was described in Sicard et al. (2006). As shown in Fig. 5, the VM detects the MH between 300 and 600 m AGL. Around noon, the ML and an aloft layer are still well disconnected. The 6th packet of lidar profiles measured between 11.39 and 12.08 UTC yields a MH at 573 m. This height is in very good agreement with the MH of 605 m measured by the radiosounding at 12.00 UTC. From 14.00 UTC on, the aloft layer of aerosols above the ML is starting to sink and join the ML. The mean error of the VM for the whole day is 12%. The ML throughout the day remains under 600 m due to the local TIBL formation and the regional large mesoscale subsidence over the Western Mediterranean.

Fig. 5 depicts the comparison between the lidar-derived MH over the Barcelona city and the six scenarios including parameterisations derived directly from MM5 and MCIP. MRF and PC non-local schemes show similar results and outline a clear tendency to overestimate the MH, with biases ranging from 40% to 72% and errors from 59% to 77%. In these scenarios, MM5 and MCIP diagnoses indicate very similar results with maximum average differences of around 30% between them. However, GS–MM5 and GS–MCIP show very strong differences reaching a factor of roughly 7 at noon, with biases of −60% and 104%, respectively as daily averages; the former one underpredicting the MH provided by lidar measurements and the latter one yielding the highest MHs of all the scenarios.

Since MRF and PC (both diagnosed and re-diagnosed) and GS–MCIP present similar over-predicted MHs, Fig. 6 shows the comparison in the whole domain between GS–MM5 and GS–MCIP. These differences are found in the whole domain, indicating the substantial uncertainties in the MH determination due to the differences in the diagnosis (TKE threshold vs. Rib method). GS–MCIP simulates MHs higher than 1500 m while it remains mainly below 500 m in GS–MM5. It is remarkable that, in the early morning, for the urban coastal area, GS–MCIP shows a higher MH than inland areas due to the enhanced warming caused by the properties of urban land-use. On the contrary, GS–MCIP simulates lower MHs at noon over the coastal urban area than inland locations. This is due to the effect of the sea breeze, with TIBL formation and mesoscale subsidence over the coast.

The different MHs in the scenarios considered highly influence the photochemical concentrations over the area of study, as shown previously. The highest O_3 1-h maximum concentration is provided by GS–MM5 parameterisation (119 $\mu g\,m^{-3}$), followed by GS–MCIP (115 $\mu g\,m^{-3}$); however, the 8-h maximum average concentration in the domain and the daily average concentration within this scenario indicate that the O_3 depletion at night in GS–MM5 is higher than in other schemes (which is indicated by the higher NO_x 8-h and daily average concentrations), and therefore the O_3 concentrations in these periods of time is not favoured in GS–MM5 respect to MRF or PC schemes (or even in the GS–MCIP

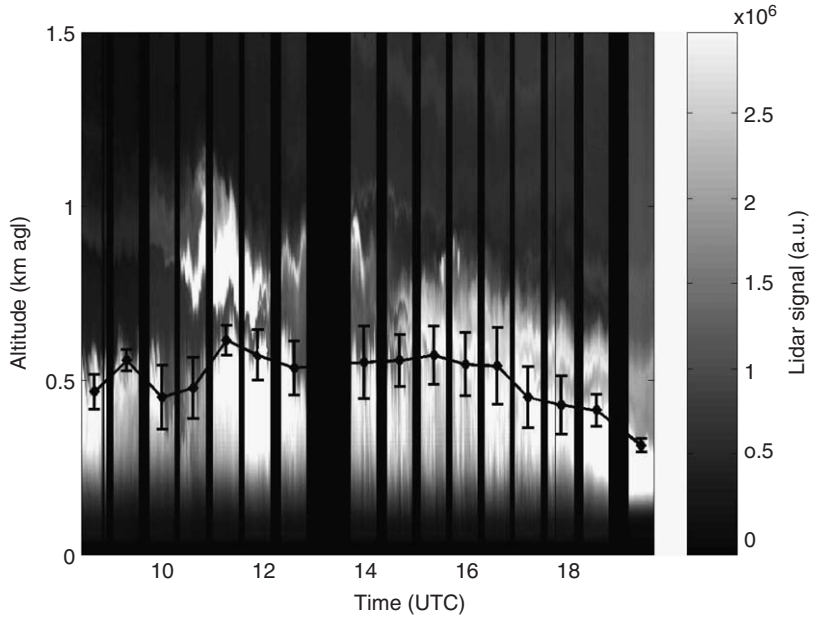

	GS-MM5	GS-MCIP	MRF-MM5	MRF-MCIP	PC-MM5	PC-MCIP
MNBE (%)	-60.12	103.89	71.92	68.56	40.20	70.30
MNGE (%)	60.12	104.64	77.41	69.31	58.59	72.64

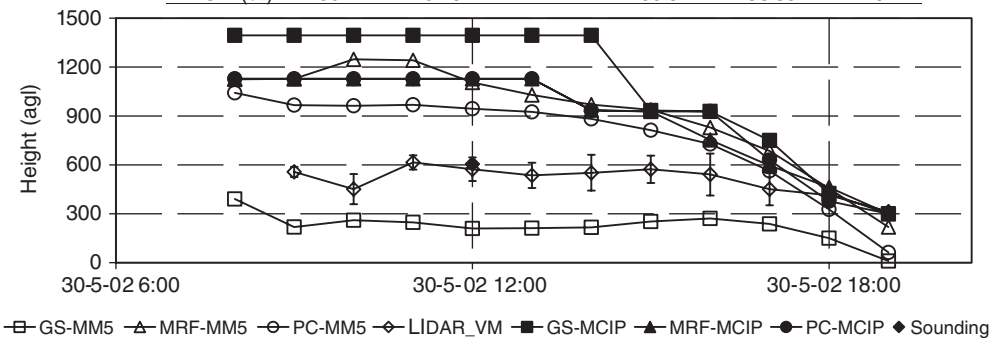

Fig. 5. (Up) Height–time display of the RSCS signal on 30 May 2002. Black asterisks represent the ML height from the lidar using the VM. The white diamond represents the ML height from the radiosounding at 1200 UTC using the Richardson number method. (Down) Evaluation and height–time display of the ML height derived from lidar, radiosounding and the three modelled PBL schemes with MM5 and MCIP diagnoses. MNBE is the mean normalised bias error and MNGE is the mean normalised gross error.

scenario). In addition, the most accurate value observed for the 1-h peak of O_3 is predicted by GS-MM5, that yields the highest values throughout the day due to the lowest MH. Despite considerably different approaches of the MH estimation for GS–MM5 and GS–MCIP, both the scenarios meet the objective of $\pm 20\%$ set by US EPA for UPA.

Another important issue is the latter peak of precursors observed in GS–MM5 (Figs. 3 for the Barcelona–Poblenou station, n.8; and Fig. 4 for the L'Hospitalet de Llobregat station, n.6) caused by the differences in the PBL development and its height among the scenarios. As stated by Jiménez et al. (2005b), the 1-h shift in peaks of precursors causes the midday emissions to produce O_3 more efficiently in Barcelona area. The higher values of NO_x reported in Table 1 for 8-h average and daily average concentrations in GS–MM5 caused by the lower MH destroys more of the available ground-level O_3 at nighttime in pervasive emission areas as cities, according to the titration reaction in which NO and O_3 combines to produce NO_2 and molecular oxygen ($NO + O_3 \rightarrow NO_2 + O_2$). The daily average concentrations of NO_x range from

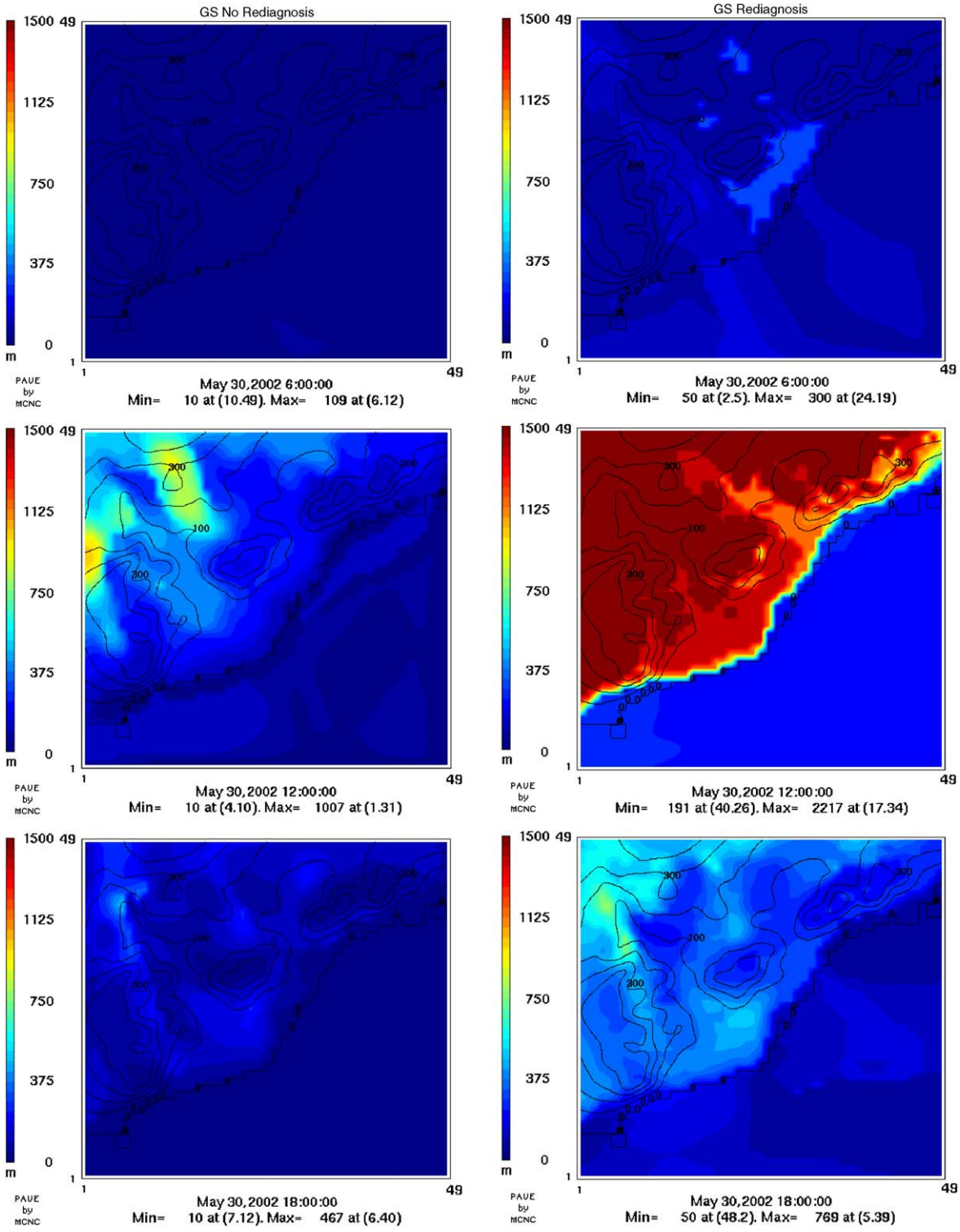

Fig. 6. PBL height (m agl) in the GS–MM5 (left) and GS–MCIP (right) schemes simulations in the domain of study at (up) 06.00 UTC, (centre) 12.00 UTC and (down) 18.00 UTC. Contour lines indicate the topography.

$30\,\mu g\,m^{-3}$ in the scenario of GS–MM5 to $22–24\,\mu g\,m^{-3}$ when the other scenarios are considered.

Thus, O_3 is suppressed more in the GS–MM5 scheme during nighttime and its formation is retarded, as observed in Figs. 2, 3 and 4. Moreover, the NO_2 formed from the O_3 titration removes radicals by the reaction $NO_2 + OH \rightarrow HNO_3$. If the precursors' peak is displaced to the right (latter peak, around 08.00 UTC), the higher concentrations of NO_x causes a enhanced production of O_3 (Heuss et al., 2003) in GS–MM5 compared with the other scenarios. This effect of timing can be a contributor when looking for the origin of the higher O_3 concentrations.

3.2.2. Temperature

The surface heating is affected by the cloud cover fraction, among other variables. An accurate estimation of cloud cover is important to reproduce the thermal and photochemical processes occurring within the PBL. Clouds are highly parameterised in MM5, with a tendency to underpredict cloud cover in the mid-troposphere and overpredict cloud cover in the PBL. Overestimation of clouds may lead to an inaccurate estimation of surface temperatures and PBL parameters (Zhang et al., 2001). In the domain of study, all schemes present very limited low cloud fractions (not shown). The assessment of the influence of cloud cover on the surface heating is beyond the scope of this contribution.

The temperatures are kept the same for MM5 and MCIP scenarios, since MCIP re-diagnoses just the PBL height. When the temperature from the PBL schemes is compared against ambient data from meteorological stations, the results indicate that all schemes tend to overestimate nocturnal temperatures (Fig. 7). At night, the inland regions remain too warm in all the three schemes, but with lower RMSE for the GS scenario. The MRF scheme simulates the lowest nocturnal temperatures, with a better model agreement on the inland and mountain stations of Fabra (n.2 in Fig. 1) and Garraf (n.5). During daytime, all schemes tend to underpredict the surface temperature, as shown in the negative bias error. GS presents the highest temperatures when assessed against ambient data, simulating a warmer surface layer than MRF and PC. Although PC incorporates a more complex land-surface model scheme, the behaviour of the model during this episode appears to have the largest deviations of the three different configurations used; they appear mainly when assessing the model against inland stations (Montmeló, n.4 and Garraf, n.5), with differences between PC simulations and measurements up to −6.5 K. The two other schemes also present larger errors in inland stations than coastal stations, mainly due to the properties of urban land-use. However, the underestimation of temperature is not so large between −2.0 (GS) and −4.0 K (MRF). It is important to remark the ability of the three schemes to model the diurnal evolution of the coastal station surface temperatures (not shown).

The effect of the higher surface temperatures in GS makes the MCIP Richardson number re-diagnose estimate a higher MH, as was previously shown in Fig. 5. Despite the GS scheme includes a simple slab surface model, it presents the most accurate behaviour of surface temperature during daytime when assessed versus ambient data, yielding warmer temperatures. The complexity of the domain of study, with a large coastal region, and several mountain coastal ranges enhances the difficulties undergone by more complex surface schemes.

Regarding the evaluation versus radiosounding data (Fig. 7), one can observe that although GS delivers the highest temperatures in the two first model layers closest to the ground, the local vertical mixing is less efficient in generating a deeper and well-mixed moist layer than the non-local schemes (MRF and PC), as seen both in the temperature and the mixing ratio profile.

In order to account for the influence of the surface temperature on the O_3 formation, a hypothetical simulation was performed taking into account the MRF's temperatures and a new scenario considering an artificial increase of 3 K in the tropospheric temperature. Although MCIP recalculates the cloud fraction (which depends on relative humidity and thus on temperature), the radiation fluxes were not modified in order to isolate the effect of temperature on air quality. The results shown in Fig. 8 indicate that the increase in the O_3 maximum 1-h concentrations over the urban area of Barcelona in MFR + 3 K scenario can reach $7.2\,\mu g\,m^{-3}$, over $21.1\,\mu g\,m^{-3}$ in the background areas, providing $8.5\,\mu g\,m^{-3}$ of O_3 increase in the entire domain. This represents an average increase of 8.5% in the city of Barcelona, 13.2% in background areas and 10.0% as an average in the domain.

As commented before, the highest 1-h peak concentration of O_3 is yielded by GS–MM5

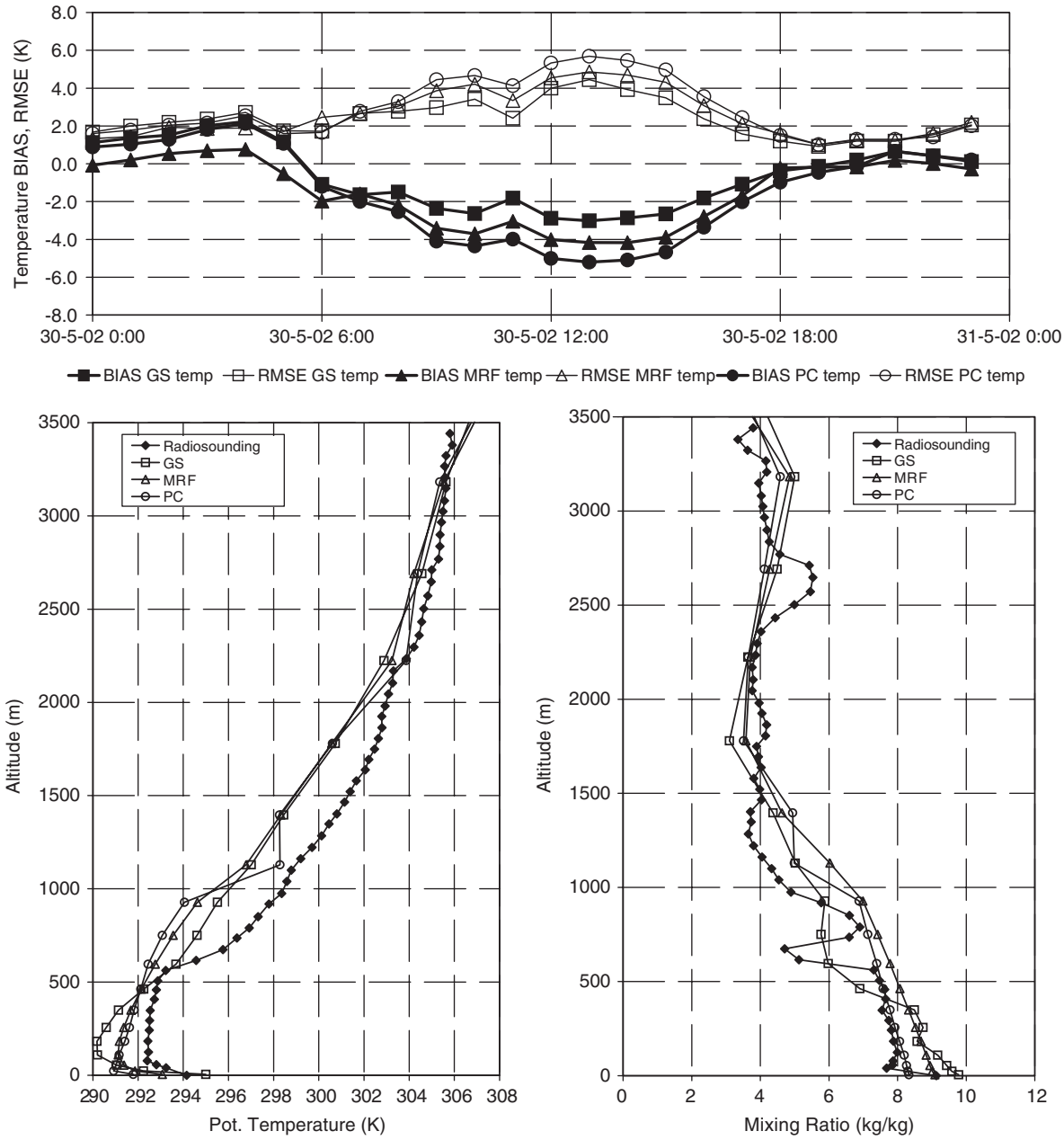

Fig. 7. Evaluation of the PBL schemes against meteorological data: (Up) daily evolution of the surface temperature bias and RMSE; (down-left) vertical potential temperature at 12.00 UTC; (down-right) vertical mixing ratio at 12.00 UTC.

parameterisation (119 $\mu g\,m^{-3}$) (Fig. 9). GS–MM5 scheme provides the lowest height of the PBL and the temperatures estimated by GS during daytime are higher than those estimated by MRF or PC, the latter providing the lowest temperature estimations in the areas where the meteorological stations are located. These areas are mainly urban areas belonging to the BGA, as was previously shown in Fig. 1. If we consider GS–MCIP (Fig. 9), where the MHs are similar and even higher to the rest of parameterisations, we found out that the GS also provides higher 1-h concentrations of O_3 (115 $\mu g\,m^{-3}$) than other scenarios (Fig. 10 for MRF and Fig. 11 for PC), as depicted in Table 1.

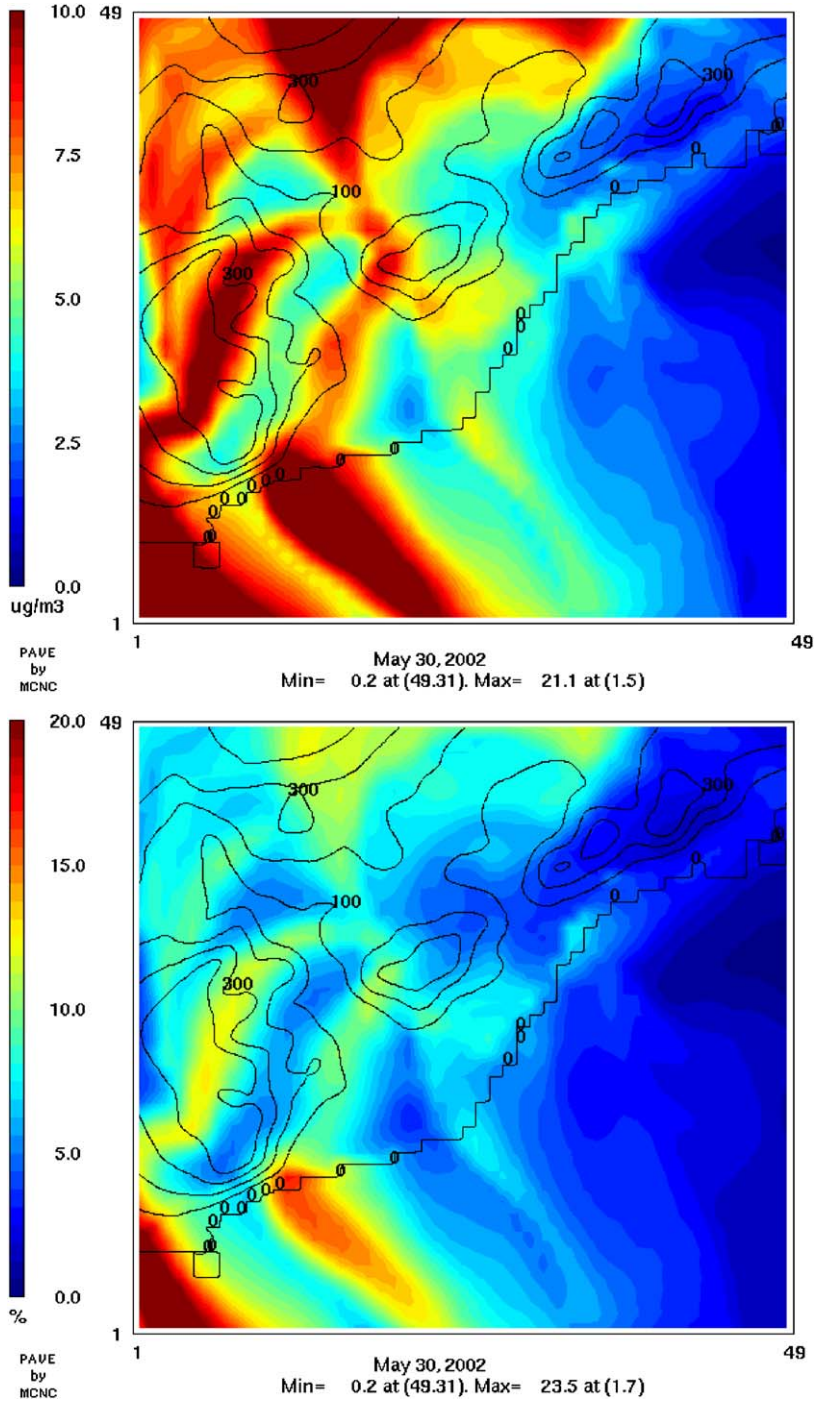

Fig. 8. (Up) Difference in the peak 1-h maximum concentrations of O_3 ($\mu g\,m^{-3}$) and (down) percentual difference (%) in the simulations with MRF + 3 K scenario minus MRF simulation in the domain of study.

Although statistics reveal that the MH diagnosis is the determinant factor in the increase of O_3 concentrations, we suggest the effect of temperature in the area of study may play a non-negligible role, as highlighted by the hypothetical scenario of MRF + 3 K.

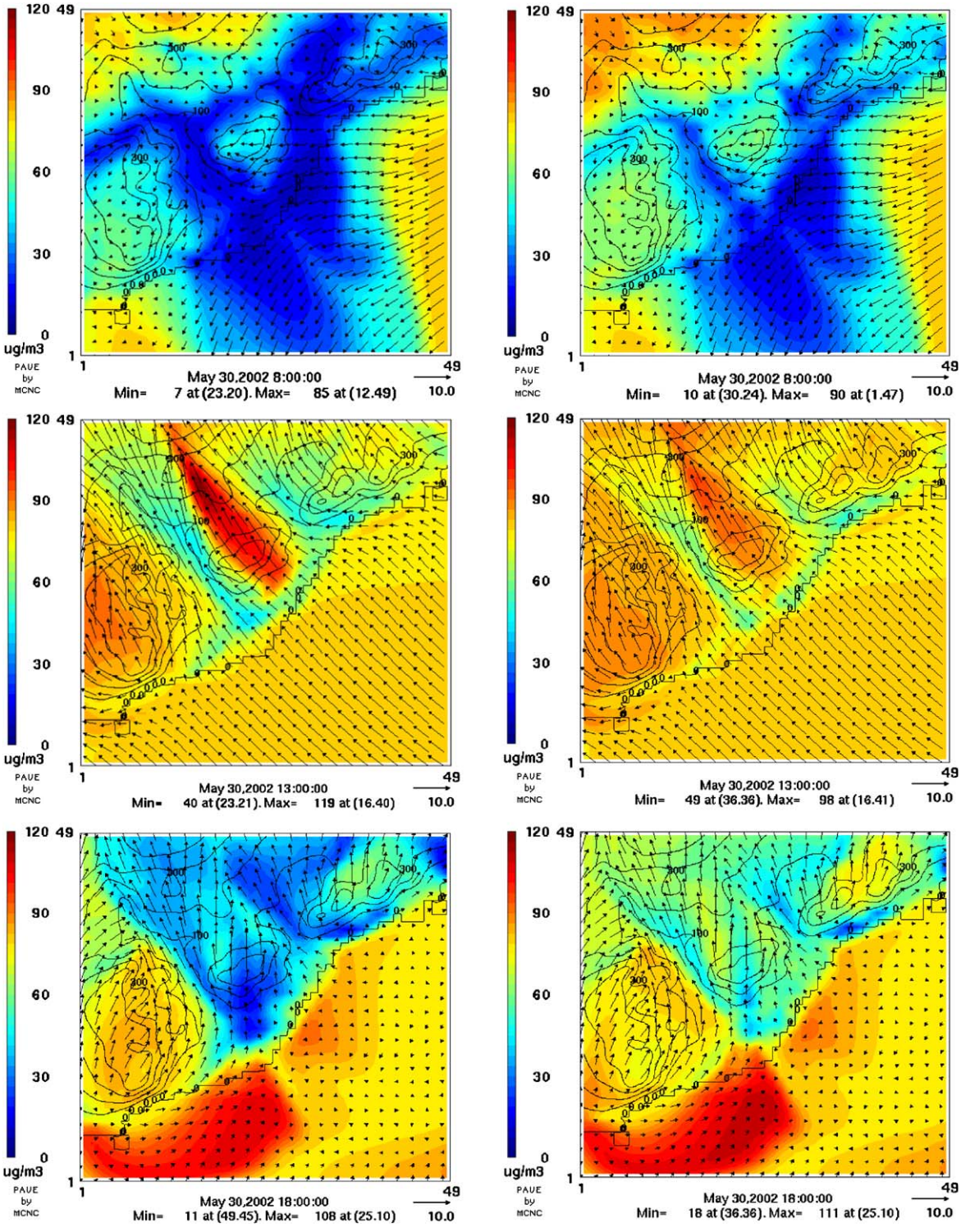

Fig. 9. Wind fields ($m\,s^{-1}$) and ground level O_3 concentrations ($\mu g\,m^{-3}$) in the GS–MM5 (left) and GS–MCIP (right) scenario at (up) 08.00 UTC, (centre) 13.00 UTC and (down) 18.00 UTC.

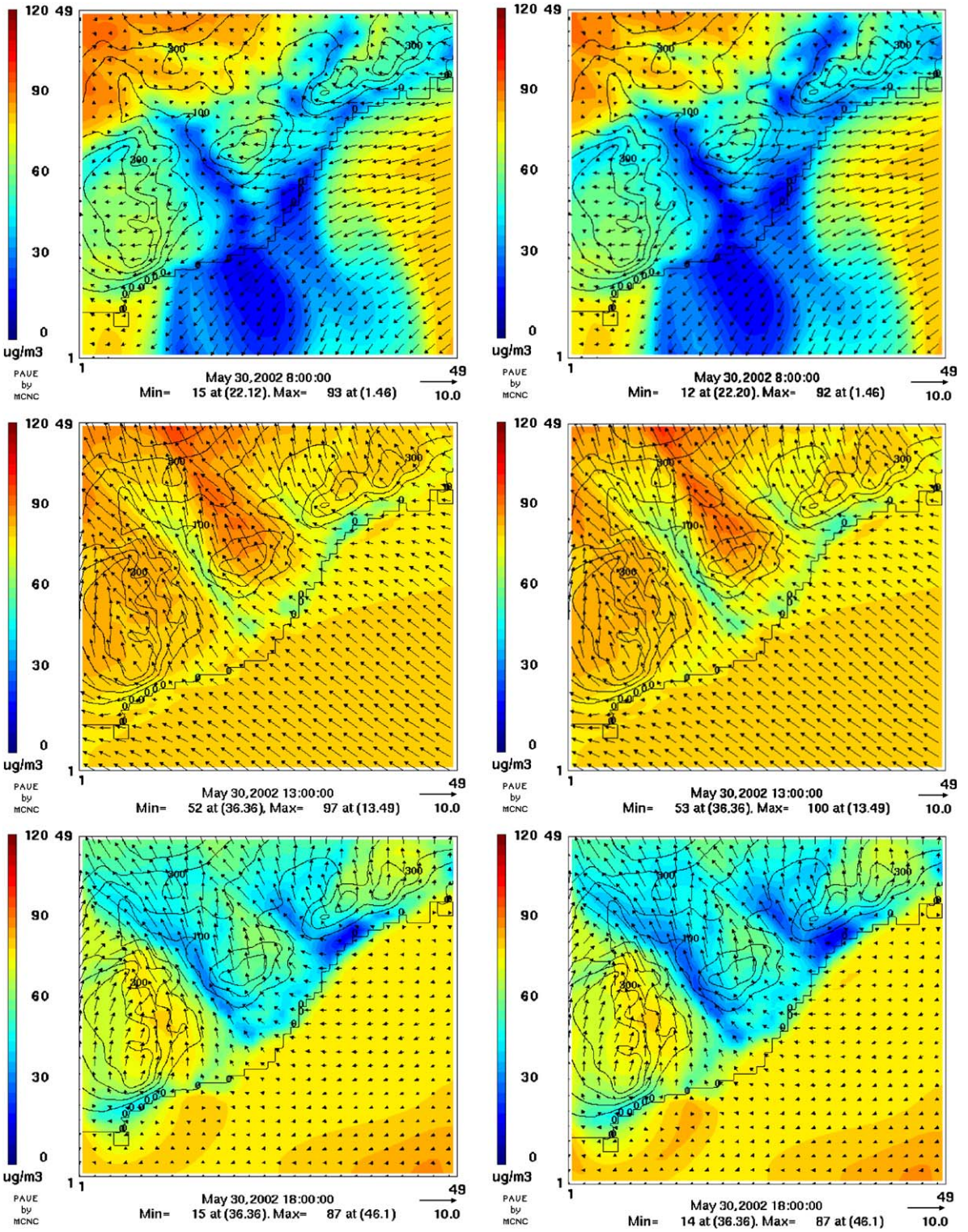

Fig. 10. Wind fields ($m\,s^{-1}$) and ground level O_3 concentrations ($\mu g\,m^{-3}$) in the MRF–MM5 (left) and MRF–MCIP (right) scenario at (up) 08.00 UTC, (centre) 13.00 UTC and (down) 18.00 UTC.

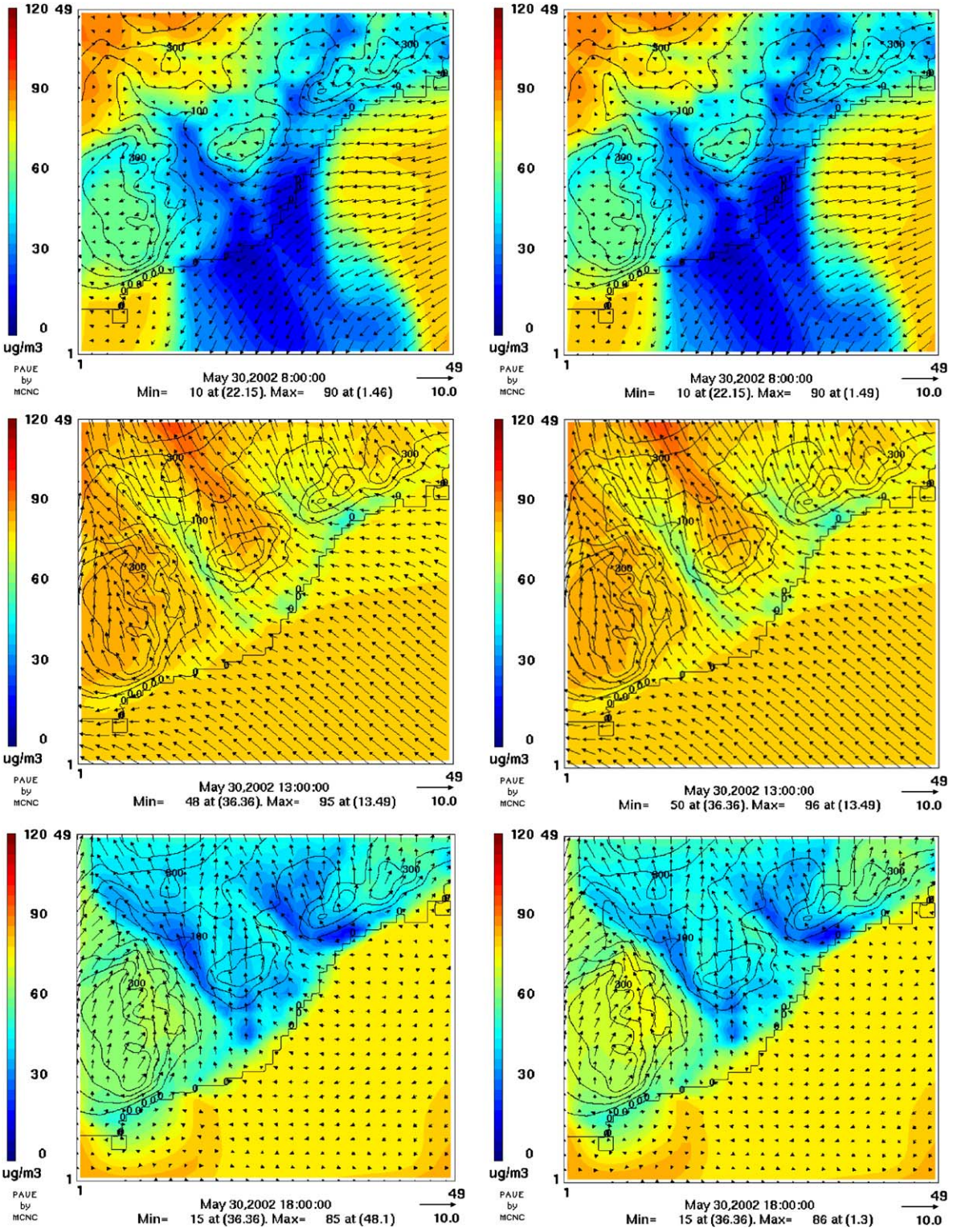

Fig. 11. Wind fields ($m\,s^{-1}$) and ground level O_3 concentrations ($\mu g\,m^{-3}$) in the PC–MM5 (left) and PC–MCIP (right) scenario at (up) 08.00 UTC, (centre) 13.00 UTC and (down) 18.00 UTC.

3.2.3. Wind speed and direction

With respect to wind fields, the statistics of wind speed (Fig. 12) show an overestimation of nocturnal winds around 1–2 m s^{-1}, with a better agreement of MRF scheme. At night, the model overestimates the wind speed over 3 m s^{-1} in Badalona station (n.3 in Fig. 1), and the error remains below 2 m s^{-1} in the other stations (not shown).

With the see breeze development, GS and MRF simulations underestimate the intensity of onshore flows, with RMSE around 1.5 m s^{-1}. Moderately better RMSE statistics are obtained with PC, though an overestimation of the speed of the flow is observed with this scheme (positive bias). The slowest daily winds are simulated with GS, followed by MRF. The stronger sea breeze in the non-local schemes can be explained by their higher vertical transport of heat flux over land, creating a larger land–sea contrast above the surface (Zhang et al., 2001). The wind direction is fairly well captured by all the three schemes during daytime with RMSE below 60° (Fig. 12). The PC scheme presents the best agreement with the meteorological stations data. GS appears to present the lowest accuracy in the prediction of wind direction but with a similar performance in the evening. The problems arise at nighttime, with an increase of the error of the model when reproducing wind direction associated to the low wind speeds. This becomes particularly evident in the change of the breeze regimes from land to sea breeze and vice versa (06.00 and 19.00 UTC), which produces erroneous wind direction values.

The general behaviour of the simulated winds at Barcelona is satisfactory when compared with the radiosounding data. The model tends to underestimate the near surface winds in the first layer of the model, especially with the GS scheme. Between 500 and 1500 m the model appears to underpredict the speed and presents a negative bias of 50–80o, while it depicts a reasonable agreement with the radiosounding above 1500 m.

As in the case of temperature, the wind fields in the different scenarios (Figs. 9, 10 and 11) also tend to differ between the schemes along the coastal and inland regions, with larger wind speed gradients predicted by the GS at night and PC during daytime hours. The weaker sea breezes forecasted by GS during daytime favour the accumulation of O_3 precursors in coastal areas (Fig. 9), and therefore O_3 is formed in different locations according to the PBL parameterisation selected. In the case of MRF (Fig. 10) and PC (Fig. 11), the O_3 and its precursors are advected out from the domain of BGA through the northern boundary. The higher concentrations of O_3 in the Garraf region over the sea (southwestern part of the area of study) provided by GS can be explained by larger wind speeds of this scheme in the area that transport O_3 from the reservoir layer of the Mediterranean inland the domain through the southern boundary. This contribution of advective transport is important for the GS simulations, opposite to the near-stagnation region reported by MRF a nd PC.

4. Conclusions

In this contribution, meteorological fields that are used as inputs to a chemical transport model are simulated in the Barcelona area with the local Gayno–Seaman (GS) coupled to a slab model, non-local Medium Range Forecast (MRF) to the five-layer soil model and non-local Pleim–Chang (PC) to the Pleim–Xiu land-surface model as diagnosed by MM5 and re-diagnosed by Meteorology-Chemistry Interface Processor (MCIP). A typical summertime situation was considered for analysing the dependency of air quality on the planetary boundary layer (PBL) scheme. A typical summertime situation was considered for analyzing the dependency of air quality on the PBL scheme.

The comparison between the lidar-derived mixing height (MH) over the Barcelona city and the scenarios including parameterisations derived directly from MM5 and MCIP indicates that non-local schemes show similar results and outline a clear tendency to overestimate the MH. However, GS–MM5 underpredicts the MH provided by lidar measurements, but GS-MCIP yields the highest MHs of all the scenarios.

During daytime, all the schemes tend to underpredict the surface temperature. GS presents the highest temperatures when assessed against ambient data, simulating a warmer surface layer than MRF and PC. The effect of the higher surface temperatures in GS makes the MCIP Richardson number re-diagnose estimate a higher MH. GS delivers the highest temperatures in the two first model layers closest to the ground; the local vertical mixing is less efficient in generating a deeper and well-mixed moist layer than the non-local schemes.

With respect to wind fields, GS simulations underestimate the intensity of onshore flows more

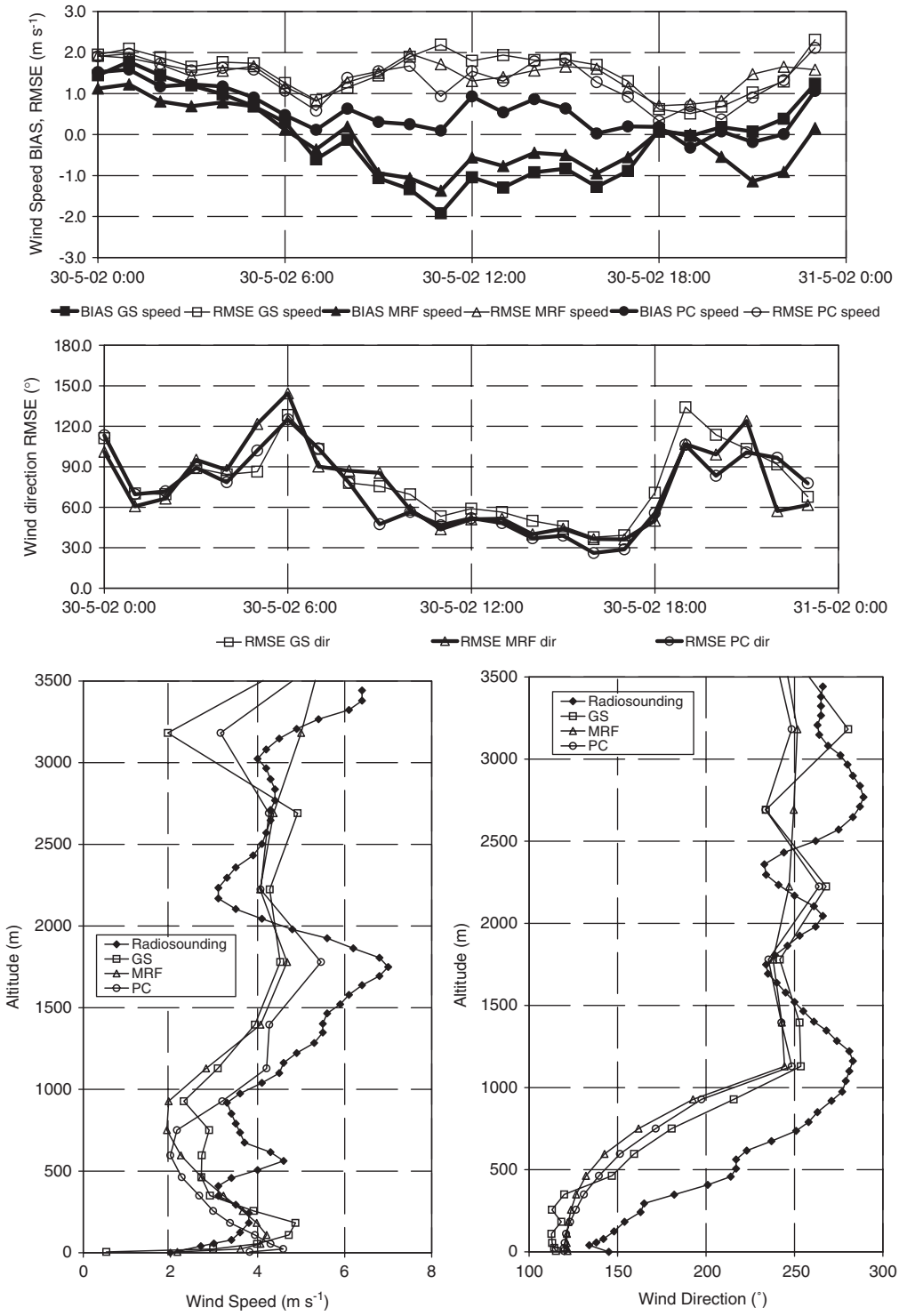

Fig. 12. Evaluation of the PBL schemes against meteorological data: (up) daily evolution of the wind speed bias and RMSE; (centre) daily evolution of the wind direction RMSE; (down-left) wind speed in the low troposphere at 12.00 UTC; (down-right) wind direction in the low troposphere at 12.00 UTC.

than the other scenarios. The stronger sea breeze in the non-local schemes can be explained by their higher vertical transport of heat flux over land, creating a larger land–sea contrast above the surface. The parameterisations become inaccurate for reproducing the wind direction when associated to low wind speeds. This is particularly evident in the change of the breeze regimes from land to sea breeze and vice versa.

The results of the air quality simulations with the different schemes indicate that modelled daily maximum 1-h O_3 and CO concentrations vary in magnitude and location in function of the PBL scheme. In addition, the GS–MM5 scenario presents the lowest MHs, the highest surface temperatures and the weakest winds during daytime, which provokes an enhanced O_3 formation. As a consequence, a shift of 1 h in peaks of precursors observed in the GS–MM5 scenario causes the midday emissions to produce O_3 more efficiently.

At night, the higher concentrations of NO_x in the GS–MM5 scheme (which are caused mainly by the lower MH) provokes a higher depletion of O_3, which yields lower concentrations of this pollutant during nighttime in downtown Barcelona.

The GS–MCIP demonstrates that although it yielded a similar or even higher MH, the 1-h peak O_3 concentrations were higher than those reported by the other schemes, highlighting the influence of temperature (despite it is a moderate influence) in air quality simulations.

From a regulatory point of view, and since the MM5–EMICAT2000–CMAQ model tends to underestimate the photochemical formation in the area of study due to an underestimation of VOCs emissions in a VOC-limited area as Barcelona, the increase in temperature shown by GS scheme, together with a lower MH by GS–MM5 and the behaviour of the winds (that allow the accumulation of O_3 and its precursors during the hours of photochemical formation) promotes the O_3 concentration in the area of study and therefore they improve the statistical results in all the scores. Therefore, important efforts should be done when configuring meteorological modelling and chemical transport pre-processors in relation to PBL schemes when performing air quality simulations. Depending on the area of study, emission estimates and chemical regimes of O_3 formation (NO_x or VOC-limited areas), significant differences may appear between the methodologies implemented in several PBL parameterisations.

Acknowledgements

This work was developed under the research contract REN2003-09753-C02 of the Spanish Ministry of Education and Science. P. Jiménez also thank this Ministry for the FPU doctoral fellowship hold. ESA and MCYT are thanked, respectively, for the external postdoctoral fellowship and the Ramón y Cajal position hold by M. Sicard. The authors gratefully acknowledge Dr. R. Parra and E. López for the EMICAT2000 emissions. Air quality stations and meteorological data were provided by the Environmental Department of the Catalonia Government (Spain).

References

Athanassiadis, G.A., Rao, S.T., Ku, J.-Y., Clark, R.D., 2002. Boundary layer evolution and its influence on ground-level ozone Concentrations. Environmental Fluid Mechanics 2, 339–357.

Baldasano, J.M., Cremades, L., Soriano, C., 1994. Circulation of air pollutants over the Barcelona geographical area in summer. In: Proceedings of Sixth European Symposium Physico-Chemical Behavior of Atmospheric Pollutants, 18–22 October, 1993, Varese (Italy). Report EUR 15609/1 EN, pp. 474–479.

Boers, R., Eloranta, E.W., Coulter, R.L., 1984. Lidar observations of mixed layer dynamics: tests of parametrized entrainment models of mixed layer growth rate. Journal of Climatology and Applied Meteorology 23, 247–266.

Byun, D.W., Ching, J.K.S. (Eds.), 1999. Science algorithms of the EPA Models-3 Community Multiscale Air Quality (CMAQ) modeling system. EPA Report N. EPA-600/R-99/030. Office of Research and Development. US Environmental Protection Agency, Washington, DC.

Byun, D.W., Pleim, J.E., Tang, R.T., Bougeios, A., 1999. Meterorology-Chemistry Interface Processor (MCIP) for Models-3 Community Multiscale Air Quality (CMAQ) modeling system. In: Byun, D.W., Ching, J.K.S. (Eds.), Science Algorithms of the EPA Models-3 Community Multiscale Air Quality System (CMAQ) Modeling System. Atmospheric Modeling Division, US Environmental Protection Agency, Research Triangle Park, NC, USA, EPA 600/R-99/030, 90pp.

Dudhia, J., 1993. A non-hydrostatic version of the Penn State-NCAR mesoscale model: Validation tests and simulation of an Atlantic cyclone and cold front. Monthly Weather Review 121, 1493–1513.

Dudhia, J., 1996. A multi-layer soil temperature model for MM5. In: The Sixth PSU/NCAR Mesoscale Model Users Workshop, 1996.

Elleman, R.A., Covert, D.S., Mass, C.F., 2003. Comparison of ACM and MRF boundary layer parameterizations in MM5. In: 2003 Models-3 Workshop, Raleigh, NC, USA.

Gayno, G., 1994. Development of a higher-order, fog-producing boundary layer model suitable for use in numerical weather

prediction. M.S. Thesis, Pennysylvania State University, 104pp.

Gery, M.W., Whitten, G.Z., Killus, J.P., Dodge, M.C., 1989. A photochemical kinetics mechanism for urban and regional scale computer modeling. Journal of Geophysical Research 94 (D10), 12925–12956.

Heuss, J.M., Kahlbaum, D.F., Wolff, G.T., 2003. Weekday/weekend ozone differences: what can we learn from them? Journal of the Air & Waste Management Association 53, 772–788.

Holtslag, A.M.M., DeBruijn, D., Pan, C., 1990. A high-resolution air mass transformation model for short-range weather forecasting. Monthly Weather Review 118, 1561–1575.

Holtslag, A.A.M., Meijgaard, E.V., DeRooy, W.C., 1995. A comparison of boundary layer diffusion schemes in unstable conditions over land. Boundary-Layer Meteorology 76, 69–95.

Hong, S.Y., Pan, H.L., 1996. Nonlocal boundary layer vertical diffusion in a Medium-Range Forecast model. Monthly Weather Review 124, 2322–2339.

Huang, H.-C., Chang, J.S., 2001. On the performance of numerical solvers for a chemistry submodel in three-dimensional air quality models. Journal of Geophysical Research 106, 20175–20188.

Jang, C.J., Jeffries, H.E., Byun, D., Pleim, J.E., 1995. Sensitivity of ozone to model grid resolution—II. Detailed process analysis for ozone chemistry. Atmospheric Environment 29 (21), 3101–3114.

Jiménez, P., Baldasano, J.M., 2004. Ozone response to precursor controls in very complex terrains: use of photochemical indicators to assess O_3–NO_x–VOC sensitivity in the north-eastern Iberian Peninsula. Journal of Geophysical Research 109, D20309.

Jiménez, P., Jorba, O., Parra, R., Baldasano, J.M., 2005a. Influence of high-model grid resolution on photochemical modeling in very complex terrains. International Journal of Environment and Pollution 24 (1/2/3/4), 180–200.

Jiménez, P., Parra, R., Gassó, S., Baldasano, J.M., 2005b. Modeling the ozone weekend effect in very complex terrains: a case study in the northeastern Iberian Peninsula. Atmospheric Environment 39, 429–444.

Kain, J.S., Fritsch, J.M., 1993. Convective parameterisation for mesoscale models: The Kain–Fritsch scheme. The representation of cumulus convection in numerical models. In: Emanuel, K.A., Raymond, D.J. (Eds.), American Meteorological Society, 246pp.

Kanamitsu, M., 1989. Description of the NMC global data assimilation and forecast system. Weather and Forecasting 4, 335–342.

Ku, J.-Y., Mao, H., Zhang, K., Civerolo, K., Rao, S.T., Philbrick, C.R., Doddridge, B., Clark, R., 2001. Numerical investigation of the effects of boundary-layer evolution on the predictions of ozone and the efficacy of emission control options in the northeastern United States. Environmental Fluid Mechanics 1, 209–233.

Millán, M.M., Salvador, R., Mantilla, E., Artíñano, B., 1996. Meteorology and photochemical air pollution in southern Europe: experimental results from EC research projects. Atmospheric Environment 30, 1909–1924.

Millán, M.M., Salvador, R., Mantilla, E., 1997. Photooxidant dynamics in the Mediterranean Basin in summer: results from European Research Projects. Journal of Geophysical Research 102 (D7), 8811–8823.

MMMD/NCAR, 2001. PSU/NCAR Mesoscale Modeling System Tutorial Class Notes and User's Guide: MM5 Modeling System Version 3.

Ntziachristos, L., Samaras, Z., 2000. COPERTIII Computer programme to calculate emissions from road transport. Methodology and emission factors (Version 2.1). Technical Report No. 49, European Environment Agency.

Parra, R., Jiménez, P., Baldasano, J.M., 2006. Development of the high spatial resolution EMICAT2000 emission model for air pollutants from the north-eastern Iberian Peninsula (Catalonia, Spain). Environmental Pollution 140, 200–219.

Pérez, C., Sicard, M., Jorba, O., Comerón, A., Baldasano, J.M., 2004. Summertime re-circulations of air pollutants over the north-eastern Iberian coast observed from systematic EARLINET lidar measurements in Barcelona. Atmospheric Environment 38, 3983–4000.

Pleim, J.E., Chang, J.S., 1992. A non-local closure model for vertical mixing in the convective boundary layer. Atmospheric Environment 26A, 965–981.

Pleim, J.E., Clarke, J.F., Finkelstein, P.L., Cooter, E.J., Ellestad, T.G., Xiu, A., Angevine, W.M., 1996. Comparison of measured and modeled surface fluxes of heat, moisture and chemical dry deposition. In: Gryning, Schiermeier (Eds.), Air Pollution Modeling and its Application XI,. Plenum Press, New York.

Pleim, J.E. , Xiu, A., Finkelstein, P.L., Clarke, J.F., 1997. Evaluation of a coupled landsurface and dry deposition model through comparison to field measurements of surface heat, moisture, and ozone fluxes. In: Proceedings of the 12th Symposium on Boundary Layers and Turbulence, 28 July–1 August 1997, Vancouver, BC.

Russell, A., Dennis, R., 2000. NARSTO critical review of photochemical models and modeling. Atmospheric Environment 34, 2283–2324.

Seibert, P., Beyrich, F., Gryning, S. E., Joffre, S., Rasmussen, A., Tercier, P., 1998. Mixing layer depth determination for dispersion modelling. In: COST Action 710—Final Report. Harmonisation of the pre-processing of meteorological data for atmospheric dispersion models, Report of Working Group 2. Office for Official Publications of the European Communities, Luxembourg.

Sicard, M., Pérez, C., Rocadenbosch, F., Baldasano, J.M., García-Vizcaino, D., 2006. Mixed-layer depth determination in the Barcelona coastal area from regular Lidar measurements: Methods, results and limitations. Boundary-Layer Meteorology 119 (1), 135–157. DOI:10.1007/s10546-005-9005-9, URL: http://dx.doi.org/10.1007/s10546-005-9005-9.

Soriano, C., Baldasano, J.M., Buttler, W.T., Moore, K., 2001. Circulatory patterns of air pollutants within the Barcelona Air Basin in a summertime situation: lidar and numerical approaches. Boundary-Layer Meteorology 98 (1), 33–55.

US EPA, 1991. Guideline for Regulatory Application of the Urban Airshed Model. US EPA Report No. EPA-450/4-91-013. Office of Air and Radiation, Office of Air Quality Planning and Standards, Technical Support Division. Research Triangle Park, NC, USA.

Viana, M., Pérez, C., Querol, X., Alastuey, A., Baldasano, J.M., 2005. Monitoring of PM levels in a complex summer

atmospheric scenario in Barcelona (NE Spain). Atmospheric Environment 39, 5343–5361.

Xiu, A., Pleim, J.E., 2001. Development of a land surface model. Part I: application in a mesoscale meteorological model. Journal of Applied Meteorology 40, 192–209.

Zhang, D.L., Anthes, R.A., 1982. A high resolution model of the planetary boundary layer sensitivity tests and comparisons with SESAME-79 data. Journal of Applied Meteorology 21, 1594–1609.

Zhang, K., Mao, H., Civerolo, K., Berman, S., Ku, J-Y., Rao, S.T., Doddridge, B., Philbrick, C.R., Clark, R., 2001. Numerical Investigation of boundary-layer evolution and nocturnal low-level jets: local versus non-local PBL schemes. Environmental Fluid Mechanics 1, 171–208.

Zilitinkevich, S.S., 1989. Velocity profiles, the resistance law and the dissipation rate of mean flow kinetic energy in a neutrally and stably stratified planetary boundary layer. Boundary-Layer Meteorology 46, 367–387.